

ly). Samples were incubated in a buffer-equilibrated humidity chamber at 46°C for 90 min, then rinsed and immersed in wash buffer [20 mM tris-HCl (pH 7.4), 0.01% SDS, 5 mM EDTA, 0.9 M to 7 mM NaCl (23)] for 15 min at 48°C. Slides were rinsed in distilled water, air dried, and mounted with Vectashield (Vectashield Laboratories) for viewing. Enrichment cultures were used to determine optimal stringency for hybridization with FER656 (5'-CGTTTAACTCAC-CCGATC-3'). The isolate fer1 was used as the positive control for hybridizations with FER656. Bacterial cultures used for negative FER656 hybridization controls included *T. ferrooxidans* (American Type Culture Collection 19859), *Acidimicrobium ferrooxidans* (German Collection of Microorganisms and Cell Cultures (DSMZ) 10331), *Acidiphilium* strain SJH (courtesy of B. Goebel), and *Escherichia coli* (JM109; purchased from Promega, WI). Bacterial and *Ferroplasma* cells in enrichment cultures were also used as controls; bacteria (*Leptospirillum ferrooxidans* and *Thiobacillus caldus*) were hybridized with BAC338 (8) (20% formamide).

14. For determination of generation times, 20 ml of medium (10) with 20 g liter⁻¹ FeSO₄·7H₂O and 0.02% yeast extract were adjusted to the appropriate

pH with H₂SO₄ and inoculated with 0.2 to 0.5 ml of a stationary phase culture. The pH electrode (Orion) was calibrated with commercially purchased standards for pH 1, 2, and 3 (Fisher Scientific) and with 0.146 M (pH 0.86), 0.734 M (pH 0.09), and 1.497 M (pH -0.38) H₂SO₄ reference solutions (24). Growth was determined by making direct cell counts with a Petroff-Hausser Counter (Fisher Scientific). Growth was not sustained above pH 2.5 or below 0. Comparable growth on 0.02% yeast extract in the absence of pyrite or FeSO₄·7H₂O is attained at pH 1.2.

15. P. L. Bond, S. P. Smirga, J. F. Banfield, unpublished data.

16. M. Vasquez, E. R. B. Moore, R. T. Espejo, *FEMS Microbiol. Lett.* **173**, 183 (1999).

17. J. T. Staley, *ASM News* **65**, 681 (1999).

18. J. L. van de Vossen and A. J. Driessen, *Extremophiles* **2**, 163 (1998).

19. C. Schleper et al., *J. Bacteriol.* **177**, 7050 (1995).

20. C. Schleper, G. Puehler, H. P. Klenk, W. Zillig, *Int. J. Syst. Bacteriol.* **46**, 814 (1996).

21. S. M. Barns, R. E. Fundyga, M. W. Jeffries, N. R. Pace, *Proc. Natl. Acad. Sci. U.S.A.* **91**, 1609 (1994).

22. P. Hugenholtz, B. M. Goebel, N. R. Pace, *J. Bacteriol.* **180**, 4765 (1998).

23. R. Lathe, *J. Mol. Biol.* **183**, 1 (1985).

24. D. K. Nordstrom, C. N. Alpers, C. J. Ptacek, *Environ. Sci. Technol.* **34**, 254 (1999).

25. B. L. Maidak et al., *Nucleic Acids Res.* **25**, 109 (1997).

26. D. A. Benson, M. S. Boguski, D. J. Lipman, J. Ostell, B. F. Ouellette, *Nucleic Acids Res.* **26**, 1 (1998).

27. Distributed by W. Ludwig and O. Strunk, University of Munich.

28. W. W. Barker, S. A. Welch, S. Chu, J. F. Banfield, *Am. Mineral.* **83**, 1551 (1998).

29. K. J. Edwards, thesis, University of Wisconsin-Madison (1999).

30. J. Kapuscinski, *Biotech. Histochem.* **70**, 220 (1995).

31. We thank D. K. Nordstrom, E. A. Webb, and the reviewers for their comments and P. Golyshin for providing us with his unpublished manuscript. We thank L. Kerr and Y. Chen for assistance with electron microscopy. We also thank Iron Mountain Mine for site access and Stauffer Management for providing assistance. Supported by NSF grant CHE-9521731.

9 November 1999; accepted 27 January 2000

Seismic Images of the Far Side of the Sun

C. Lindsey^{1*} and D. C. Braun^{1,2}

Images of an active region on the far side of the sun were derived by applying seismic holography to recent helioseismic observations from space. Active regions are the centers of energetic phenomena such as solar flares and coronal mass ejections, whose resulting electromagnetic and particle radiation interfere with telecommunications and power transmissions on Earth and can pose significant hazards to astronauts and spacecraft. Synoptic seismic imaging of far-side solar activity will now allow anticipation of the appearance of large active regions more than a week ahead of their arrival on the east solar limb.

Forecasts of space weather would be greatly improved by the ability to monitor active regions on the far side of the sun. Active regions on the near solar surface produce flares that affect spacecraft, cause surges in electrical power grids, and inhibit telecommunications. Because the sun rotates rapidly, with a synodic period of 27 days, flaring regions can appear suddenly on the east solar limb, affecting space weather in the terrestrial neighborhood as they pass across the near solar surface. Many such regions could be anticipated by a week or more if we could effectively monitor the far surface of the sun.

Helioseismic holography was proposed a decade ago (1) as a general diagnostic basis for local helioseismology, with the purpose of imaging local acoustic anomalies in the solar interior and on the far side. The development of holographic seismic imaging techniques for solar interior diagnostics (2, 3) was initially prompted by the discovery that sun-

spots absorb (4, 5) and scatter (6) incident acoustic waves. Phase-coherent seismic imaging opened the possibility of detecting not only local magnetic and thermal structure beneath the solar surface, but even active regions on the far side of the sun (1). These techniques work because the solar interior is transparent to seismic waves. We developed the basic concepts for seismic holography for these purposes (1, 2, 7), reviving a concept originally proposed some 15 years earlier by Roddier (8).

Standard holographic imaging of the near solar interior is accomplished computationally by regressing surface acoustic wave disturbances, which are determined by helioseismic observations, backward into the interior, on the basis of a computational acoustic model of the solar interior (9), thereby expressing a field called the coherent acoustic egression, H_+ (10). Generally, the surface observations that contribute to the regressed acoustic field at any given "focal point" in the image are chosen from a limited region, called the pupil of the computation. This has typically been an annulus or circular region on the model surface centered directly above the submerged focal point. In fact, waves in the 2.5- to 4.5-mHz frequency range undergo a spec-

ular reflection at the solar surface, penetrating back into the interior where they are eventually refracted back to the surface thousands of kilometers further from the source. Multiple-skip holography based on this phenomenon thus facilitates imaging of active regions from pupils far extended from the focal point. Indeed, it is even possible to extend the pupil of a holographic computation from the focal point to the opposite side of the sun. In such an application, it is the focal point that must lie on the far surface of the sun because the pupil itself must lie on the near surface in order to be directly observed. This is the principle of far-side helioseismic holography.

Standard acoustic power holography is accomplished by mapping the egression power, $|H_+|^2$, which may be integrated over time and/or temporal frequency for improved statistics. This diagnostic is sensitive to acoustic sources and absorbers, the latter of which are rendered as silhouettes. Alternatively, phase-sensitive holography (7) can be used to gauge travel-time perturbations, Δt , caused by refractive anomalies, or to gauge the magnetic depressions of sunspots and plages (11). This technique is based on phase correlations between the acoustic egression and its time-reverse counterpart, the acoustic ingression H_- , which is a coherent representation of waves that happen to be converging into the focal point, as opposed to waves emanating from it. This is the natural adaptation of time-distance correlation measurements (12, 13) to holographic reconstruction.

Here, we used two-skip phase-sensitive holography to map travel-time perturbations of the far side of the sun over a spectral range of 2.5 to 4.5 mHz. We analyzed a 24-hour interval of full-disk Dopplergrams, starting on 28 March 1998 07:00 UT, made by the Solar Oscillations Investigation-Michelson Doppler Imager (SOI-MDI) aboard the Solar Heliospheric Observatory (SOHO) spacecraft (14). We computed two-skip egression and

¹Solar Physics Research Corporation, Tucson, AZ 85718, USA. ²NorthWest Research Associates Inc., Colorado Research Associates Division, Boulder, CO 80301, USA.

*To whom correspondence should be addressed. E-mail: lindsey@sprc.com

REPORTS

ingression maps over the spectral range of 2.5 to 4.5 mHz, using a near-side pupil spanning a range from 115° to 172° from the focal point (Fig. 1). Such a configuration effectively filters the egression computation for waves whose spherical harmonic indices, ℓ , are mostly confined to a well-defined range (15). At 3.5 mHz, for example, the pupil illustrated in Fig. 1 samples waves with ℓ predominantly in the range of 22 to 40. This imposes a diffraction limit of $\sim 10^\circ$ of longitude at the solar equator, easily resolving a moderately large plage. The computations made here were devised to image an area on the solar far side that included a large, multipolar magnetic region, NOAA AR 8194 (16), which we reference to Carrington longitude 29.8° and latitude -22.8° , about 18 hours before its passage through the far-side meridian. The result is a signature that renders the active region on the far side of the sun by a local reduction in the one-way sound-travel time of about 6 s over an area covering about 300 degree² (Fig. 2A). This is consistent with the sign and magnitude of signatures that typically characterize plages imaged on the near side of the sun (17).

When the aforementioned computation

was repeated over the 24-hour interval beginning 29 March 1998 10:40 UT and centered at the same Carrington coordinates so as to follow solar rotation, the signature recurred (Fig. 2B). During this time, the region passed through the far-side meridian and appears to have been growing rapidly. The NSO/Kitt Peak magnetogram (18) of 8 April 1998, when projected onto the same Carrington coordinates as the sound-travel time maps, shows the magnetic region 10 days later, now on the near side of the sun just inside the east limb (Fig. 2C). Control computations to test the effects of near-side magnetic regions in the computational pupil show no artifacts of large near-side active regions at their far-side antipodes or thereabout (19).

The seismic imaging of the far side of the sun has important implications for research on the acoustic properties of the sun's magnetic regions and of the sun as a whole. The far-side images directly demonstrate the influence of active regions on global modes. Because these waves travel from the near side of the sun to the far side and back, they interfere with their multiple reflections. The result is a standing wave with a sharply defined frequency, called a *p*-mode, similar to

the harmonics that resonate in an organ pipe. An active region can be likened to a subtle dent in the organ pipe, slightly reducing its internal volume and thereby slightly raising its resonant frequency. As in the organ pipe, the resonant frequencies of solar *p*-modes can essentially be regarded as independent of which side of the resonant cavity the active region is on. Thus, the same acoustic perturbations that are largely or perhaps entirely

Fig. 1. Cross section of the solar interior showing the wave configuration for two-skip far-side seismic holography. Wavefronts emanating from a far-side point source (focal point) at intervals of 286 s (1/3.5 mHz) within the corridor of trajectories that are shown reflect once from the solar surface (right and left sides) and arrive in an annular pupil on the near surface (bottom) of the sun. Waves coherently emanating from the focal point (green arrows) are represented by the acoustic egression, reconstructed for each focal point in the image from the surface disturbance it creates on the near surface. Its time-reverse signature, the ingression (yellow arrows), represents identical waves coherently converging into the focal point to contribute to the local disturbance there. A local acoustic depression at the focal point will shift the phase of the ingression-egression correlation. In the case of a quasi-specular reflection at the focal point, the outside of the ingression pupil on one side (red part of wavefronts) correlates with the outside of the ingression pupil on the other (also red). Likewise for the inside of the pupil (blue part of wavefronts). Thus, the loss of either side of the pupil destroys the phase correlation for the entire pupil. For this reason, phase-sensitive holography of far-side solar activity is only practical for regions within $\sim 50^\circ$ of the antipode of disk center. The dotted circle indicates the depth of the base of the solar convection zone.

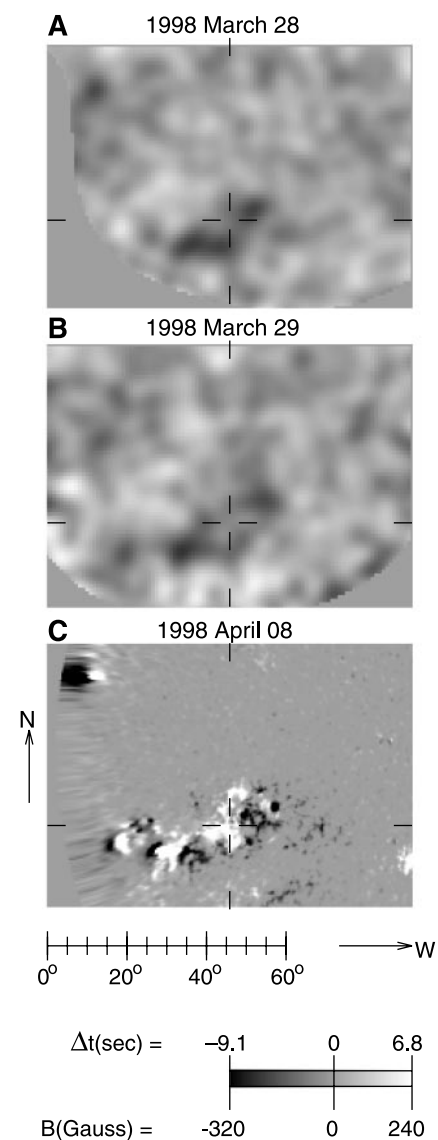
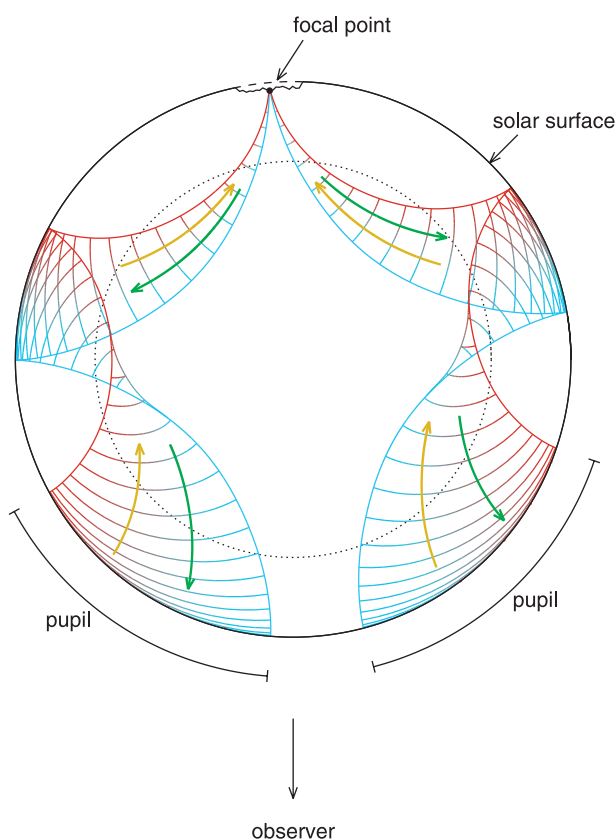


Fig. 2. Maps of one-way sound-travel time perturbation, Δt , in the neighborhood of NOAA AR 8194 just before (A) and during (B) its passage through the far-side solar meridian. Vertical fiducials in the center of each frame mark Carrington longitude 29.78° . Horizontal fiducials cross that meridian at solar latitude -22.82° . (C) An NSO/Kitt Peak magnetogram of the same location 10 days later, as the magnetic region becomes visible just inside the east limb. All three maps are overhead-view Postel projections centered on the aforementioned reference location with radial distance from the reference point indicated by the rule just beneath the bottom frame.

responsible for shifting the resonant frequencies of solar p -modes can be used to locate images of active regions on the far side of the sun when these modes are treated from the local optical perspective of seismic holography. Therefore, the far-side images reinforce a growing consensus (20, 21) that reduced sound-travel times in active regions may explain the entirety of the frequency shifts of global p -modes with the solar cycle.

The application of seismic holography to active regions on the far side of the sun makes it possible to study how active regions absorb, emit, and scatter low- ℓ waves. Plain acoustic power holography of near-side active regions renders both sunspots and plages with strong egression power deficits, comparable in significance to the phase shifts. Acoustic power holography of far-side active regions renders an unexpectedly weak signature, which is not clearly detectable in our computations. Therefore, we see that the deficit in acoustic noise radiating from plages (6, 22, 23) is substantially selective in favor of high- ℓ p -modes. This remarkable development seems tentatively consistent with recent work that attributes the acoustic egression deficit of waves emanating from magnetic regions to the coupling of p -modes with slow Alfvén modes (24, 25). Low- ℓ p -modes are characterized by mostly vertical motion, and thus couple only weakly to vertical magnetic fields.

References and Notes

1. C. Lindsey and D. C. Braun, *Sol. Phys.* **126**, 101 (1990).
2. D. C. Braun *et al.*, *Astrophys. J.* **392**, 739 (1992).
3. C. Lindsey *et al.*, in *GONG 1992: Seismic Investigation of the Sun and Stars* (Astronomical Society of the Pacific, San Francisco, CA, 1993), pp. 81–84.
4. D. C. Braun *et al.*, *Astrophys. J.* **335**, 1015 (1988).
5. T. J. Bogdan *et al.*, *Astrophys. J.* **406**, 723 (1993).
6. D. C. Braun, *Astrophys. J.* **451**, 859 (1995).
7. C. Lindsey and D. C. Braun, *Astrophys. J.* **485**, 895 (1997).
8. F. Roddier, *C. R. Hebd. Seances Acad. Sci. Ser. B* **281**, 993 (1975).
9. J. Christensen-Dalsgaard *et al.*, *Astrophys. J.* **403**, L75 (1993).
10. C. Lindsey and D. C. Braun, *Sol. Phys.*, in press; see §3, equation 1, therein.
11. Plages are magnetic regions whose flux densities, ranging from 100 to 1200 G, are considerably greater than those of the quiet sun (up to 100 G) but considerably less than those of sunspots (1200 to 3000 G). Plages viewed near the center of the solar disk are nearly invisible against the quiet sun in white light, but near the limb are about 5% brighter than the quiet sun. The strong magnetic fields of sunspots visibly depress their umbrae more than 200 km beneath level of the quiet photosphere. The reduced travel times of plages may be the result of a similar, but smaller, depression by their weaker magnetic fields.
12. T. L. Duvall Jr. *et al.*, *Nature* **362**, 430 (1993).
13. T. L. Duvall Jr. *et al.*, *Nature* **379**, 235 (1996).
14. P. H. Scherrer *et al.*, *Sol. Phys.* **162**, 129 (1995).
15. See §4 in (10).
16. The National Oceanic and Atmospheric Administration (NOAA), a branch of the U.S. Department of Commerce, monitors solar activity and assigns numbers to each major sunspot group. These are published in a periodical, *Solar Geophysical Data*, printed monthly by NOAA.
17. D. C. Braun and C. Lindsey, *Sol. Phys.*, in press.
18. The National Solar Observatory (NSO) operates solar

- telescopes at the Kitt Peak National Observatory near Tucson, AZ, and at the Sacramento Peak Observatory near Cloudcroft, NM. NSO runs a synoptic program at the Kitt Peak Vacuum Telescope that provides daily magnetograms covering the full solar hemisphere that is directly visible from the Earth. These are made available at www.nso.noao.edu/diglib.
19. Supplemental material is available at www.sciencemag.org/feature/data/1047789.shl.
20. R. Howe *et al.*, *Astrophys. J.* **524**, 1084 (1999).
21. B. W. Hindman *et al.*, *Sol. Phys.*, in press.
22. C. Lindsey and D. C. Braun, *Astrophys. J.* **499**, L99 (1998).
23. D. C. Braun, *et al.*, *Astrophys. J.* **502**, 968 (1998).

24. P. S. Cally and T. J. Bogdan, *Astrophys. J.* **486**, L67 (1997).
25. P. S. Cally, *Sol. Phys.*, in press.
26. We greatly appreciate the support we have gotten from P. Scherrer, an early and enthusiastic proponent of far-side imaging, and from the SOHO SOL-MDI team. SOHO is a project of international cooperation between the European Space Agency and NASA. Supported by NSF grants ATM-9214714 and AST-9528249, by NASA grant NAG5-7236, and by a research contract, PY-0184, sponsored by Stanford University.

8 December 1999; accepted 3 February 2000

Extreme Oxygen Sensitivity of Electronic Properties of Carbon Nanotubes

Philip G. Collins,* Keith Bradley, Masa Ishigami, A. Zettl†

The electronic properties of single-walled carbon nanotubes are shown here to be extremely sensitive to the chemical environment. Exposure to air or oxygen dramatically influences the nanotubes' electrical resistance, thermoelectric power, and local density of states, as determined by transport measurements and scanning tunneling spectroscopy. These electronic parameters can be reversibly "tuned" by surprisingly small concentrations of adsorbed gases, and an apparently semiconducting nanotube can be converted into an apparent metal through such exposure. These results, although demonstrating that nanotubes could find use as sensitive chemical gas sensors, likewise indicate that many supposedly intrinsic properties measured on as-prepared nanotubes may be severely compromised by extrinsic air exposure effects.

Many carbon materials have excellent molecular adsorption and sieving properties (1). Carbon nanotubes in particular, because of their size, large surface area, and hollow geometry, are being considered as prime materials for gas adsorption (2–4), Li storage (5, 6), and selective molecular filtering (7, 8). Independently, the results of numerous theoretical and experimental studies suggest that single-walled carbon nanotubes (SWNTs) behave as nearly ideal one-dimensional quantum wires (9–12). However, virtually no attention has been given to the possible interdependence of gas adsorption and electrical quantum conductance in nanotubes, despite the large surface area of these materials.

We show here that the measured electronic properties of nanotubes [electrical resistance R , thermoelectric power S , and local density of states $N(E)$] are in fact exceedingly sensitive to environmental conditions, namely gas exposure (13), and can be reversibly "tuned" simply by exposure to air or oxygen. Isolated, apparently

semiconducting nanotubes can be converted into apparent metals through room-temperature exposure to oxygen. Hence the electronic properties of a given nanotube are not specified only by the diameter and chirality of the nanotube but depend critically on gas exposure history. Because virtually all previous experimental studies of SWNTs have used samples exposed to air (and perhaps to other contaminants as well from aqueous solution purification or cutting processes), the results of those measurements must be carefully reevaluated before firm conclusions are drawn, especially with respect to the theoretically predicted behavior of idealized pure nanotubes.

The SWNTs used in our experiments were grown by the conventional laser ablation method (14). Material from different synthesis runs yielded similar results. In general, SWNT-rich material taken directly from the growth chamber was baked in air at 700°C to remove the majority of amorphous and microcrystalline carbon. In determining both transport and spectroscopy characteristics, different additional sample preparation and contacting procedures were used and compared in order to quantify nanotube modifications that might arise, for example, from the commonly used practices of ultrasound exposure, filtering, and surfactant addition.

Measurements of the dc electrical resistance R and thermoelectric power (TEP) S

Department of Physics, University of California at Berkeley, and Materials Sciences Division, Lawrence Berkeley National Laboratory, Berkeley, CA 94720, USA.

*Present address: IBM T. J. Watson Research Center, Post Office Box 218, Yorktown Heights, NY 10598, USA.

†To whom correspondence should be addressed. E-mail: azettl@physics.berkeley.edu